Titanium Defective Sites in TS-1: Structural Insights by Combining Spectroscopy and Simulation

Titanium defective sites in TS-1: structural insights by combining spectroscopy and simulation

Matteo Signorile,[a]§* Luca Braglia,[b]§ Valentina Crocellà,[a] Piero Torelli,[b] Elena Groppo,[a] Gabriele Ricchiardi,[a] Silvia Bordiga,[a] Francesca Bonino[a]

In memory of Professor Carlo Lamberti.

[a] Dr. Matteo Signorile, Dr. Valentina Crocellà, Prof. Elena Groppo, Prof. Gabriele Ricchiardi, Prof. Silvia Bordiga, Prof. Francesca Bonino
Department of Chemistry, NIS and INSTM Reference Centre
Università di Torino
Via G. Quarello 15, I-10135 and Via P. Giuria 7, I-10125, Torino, Italy
E-mail: matteo.signorile@unito.it
[b] Dr. Luca Braglia, Dr. Piero Torelli
TASC Laboratory
IOM-CNR
S.S. 14 km 163.5, Basovizza, I-34149 Trieste, Italy
§ MS and LB equally contributed
Supporting information for this article is given via a link at the end of the document.

Abstract

Ti silicates, and in particular Titanium Silicalite-1 (TS-1), are nowadays important catalysts for several partial oxidation reactions in the presence of aqueous H_2O_2 as oxidant. Despite the numerous studies dealing with this material, some fundamental aspects are still unfathomed. In particular, the structure and the catalytic role of defective Ti sites, other than perfect tetrahedral sites recognized as main active species, has not been quantitatively discussed in the literature. In this work, we assess the structural features of defective Ti sites on the basis of electronic spectroscopies outcomes, as interpreted through quantum-mechanical simulation. We disclose here strong evidences that the most common defective Ti sites, often reported in the TS-1 literature, are monomeric Ti centers, embedded in the zeolite framework, having a distorted octahedral local symmetry.

Introduction

Titanium Silicalite-1 (TS-1) is a synthetic zeotype,[1] whose peculiarity is the presence of Ti atoms isomorphously substituting the Si ones at tetrahedral framework positions. Despite such a sharp definition, real TS-1 samples are often characterized by the presence of different Ti sites, ranging from extended TiO_2 phases down to defective Ti sites. The “defective Ti” label covers a broad range of possible Ti moieties, whose structural description is in most of the cases barely qualitative in the literature. An increasing number of reports dealing with defective Ti sites is found in the literature appeared in the

last decade, correlated to the increasing interest toward their reactivity. TS-1 (and more generally Ti zeolites) are in fact nowadays the most relevant catalysts for propylene epoxidation[2–6] and cyclohexanone ammoximation,[7,8] and have been proposed also for the partial oxidation of other substrates.[9–12] In particular, in the framework of propylene epoxidation, the role of defective Ti is not fully clarified: it has been in fact reported to have both detrimental or incremental effect on the catalyst activity,[2,13–15] whereas it is often ascribed to a reduction in the selectivity of the catalytic reaction.[2,13] Defective TS-1 samples can originate by controlling the synthetic, as well as can be generated via post-synthetic treatments. An example of the former case was discussed by Su et al.,[15] who reported as an increase in the Na^+ concentration in the TS-1 gel during synthesis produces a higher number of defects in the final material. Post-synthetic methods instead rely on etching agents (such as ammonium hydroxide[15] or ammonium fluoride[13]) to generate the defects starting from a perfect TS-1. The group of prof. Li first attempted a structural description of defective sites by means of DR UV-Vis and UV-Raman spectroscopies, inferring that the red-shift in the LMCT transition is ascribed to an increased number of ligands in the Ti first coordination shell. They proposed as possible structure (also on the basis of DFT simulations) a bipodal Ti center, whose octahedral ligand sphere is completed by two titanol (Ti-OH) groups and two ancillary water molecules.[13] Su et al. proposed the presence of short chains of corner sharing octahedral Ti sites, on the basis of the comparison of the spectroscopic observables with those of ETS-10 and other Ti silicates, referring to them as amorphous Ti species.[15] Beside the increased number of ligands, this model proposes a higher nuclearity of the Ti defective species, involving at least two Ti atoms. Interestingly, similar dimeric structures are common in the homogenous epoxidation catalysts, such as the Sharpless catalyst.[16] More recently, Zuo and coworkers proposed the existence of lower coordinated, monomeric defective sites (namely pentahedral), also claiming their superior activity in epoxidation of propene.[14] Despite the recognition of the qualitative structural features of the defective Ti sites, their exact and univocal description is missing. A conventional approach, via comparison of the spectroscopic fingerprints of defects with those of reference materials, is hampered by the lack of well-characterized and easily accessible materials where Ti^{4+} has coordination higher than the tetrahedral, is still isolated form other metals centers and only possesses O as first neighbors. In this regard, a powerful way-through is represented by simulation of the spectroscopic properties of opportune Ti site models. Furthermore, the relation between the defective Ti site and the MFI framework can be directly considered, e.g. by adopting periodic models for the defective sites in simulations. In this work, we combine experimental and theoretical approaches, aiming to unravel the exact structure ofdefective Ti sites, while carefully accounting for their insertion in the MFI framework of TS-1. In detail, we report the outcomes from electronic spectroscopies (namely UV-vis, Ti K-edge XAS and $L_{2,3}$-edges NEXAFS, experimental details provided in Section S1.1 of SI, including the Ti K-edge XAS data extraction procedure depicted in Figure S1) compared to simulation results, allowing a comprehensive electronic description of potential defective Ti sites to be correlated to their structure.

Results and Discussion

The TS-1 samples here adopted are industrial catalysts provided by Evonik Industries AG and have been fully characterized in a previous work.[2] In detail, we focus on samples named herein as TS-1A, characterized by only perfect tetrahedral Ti sites, and TS-1B, containing a closely monodispersed population of Ti defective sites beside tetrahedral ones. The main features of the two materials, characterized by similar morphological and compositional properties, are shown in Table 1.

Table 1. Specific surface areas (SSA), Ti loading and speciation of the two samples adopted in this work.[a]

Sample	SSA (m^2g^{-1}) Langmuir	BET	wt% TiO_2 tot	wt% TiO_2 perfect	wt% TiO_2 anatase	wt% TiO_2 defective
TS-1A	573	430	2.44	2.44 (1.00)[b]	0.00 (0.00)[b]	0.00 (0.00)[b]
TS-1B	663	496	2.89	2.57 (0.89)[b]	0.12 (0.04)[b]	0.20 (0.07)[b]

[a] Data from Ref. [2]. [b] Values in brackets report the fraction of a given Ti specie over the total Ti amount.

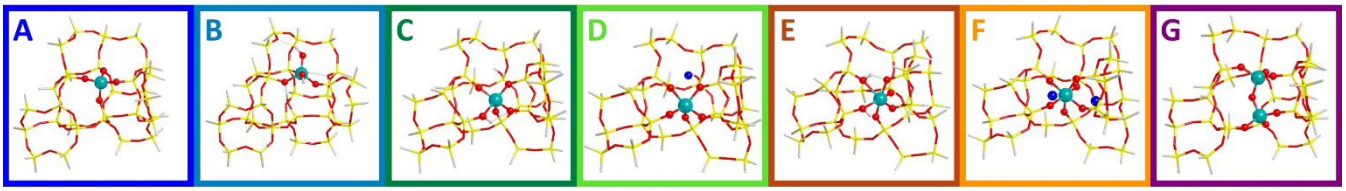

Figure 1. Cluster models (derived from the periodic structures available in the SI) for: A, perfect tetracoordinated Ti; B, bipodal tetracoordinated Ti; C, H-terminated pentacoordinated Ti; D, Na-terminated pentacoordinated Ti; E, H-terminated hexacoordinated Ti; F, Na-terminated hexacoordinated Ti; and G, dimeric tetracoordinated Ti. Atoms color code: H grey, O red, Na blue, Si yellow and Ti cyan.

Figure 1 shows the structural models of defective sites adopted in calculations reported in the following. All these structures are derived from the perfect tetrahedral Ti model sitting in the T10 site of MFI framework (model A), found to be the most favored substitutional site within the adopted computational level.[17] The full computational details, based on previous studies,[17,18] are provided in Section S1.2 of SI. The simplest defective structure (model B) was obtained by hydrolyzing two of the four Ti–O bonds connecting Ti to the framework, thus obtaining a bipodal Ti, still tetracoordinated due to the insertion of two titanol groups. The dangling Si–O were converted in Si–OH, scarcely interacting with Ti, that donate H-bonds to neighboring oxygen atoms. In order to incorporate stable hexacoordinated Ti species still bound to the MFI framework (models E-F), a Si–O unit adjacent to Ti was removed, so that Ti is forced to directly interact with six framework oxygen atoms. The excess of negative charge was balanced by introducing cations, specifically two H^+, directly bound to first-shell oxygens, or two Na^+, sitting in the neighboring small cages of MFI framework. Beside the straightforward choice of H^+ as counterion, we included also Na^+ since: i) it is a common impurity in inorganic synthesis; ii) ETS-10, characterized by extended nanowires of octahedral Ti, has Na^+ (and K^+) as counterion;[19] and iii) Su et al. showed the presence of Na^+ in the TS-1 synthetic medium promotes the formation of defects.[15] The

pentacoordinated models were derived from the H-terminated hexacoordinated (model E) by reverting a Si–OH group directly interacting with Ti in the opposite zeolite channel. As previously, both H^+ and Na^+ charge balanced structures were considered (models C and D respectively). Finally, we considered a dimeric tetrahedral Ti structure (model G), as inspired by homogenous Ti-based epoxidation catalysts.[16] Concerning the local structure of Ti, the perfect tetrahedral model A shows almost equivalent Ti–O distances (in average 1.81±0.01 Å). This value nicely reproduces the experimental outcomes from previous EXAFS studies.[20,21] A similar value is found for the average Ti–O distance in both the tetrahedral bipodal (model B) and the tetrahedral dimeric (model G) structures, being 1.81±0.03 Å and 1.80±0.01 Å respectively. Conversely, the Ti–O distance expands by increasing the number of ligands, up to 1.9±0.2 Å for the H-terminated pentacoordinated (model C) and 2.0±0.2 Å for the H-terminated hexacoordinated (model E) structures. The high standard deviation also testifies the heterogeneity in their Ti–O bond lengths, as they span among 1.81-2.19 Å and 1.83-2.36 Å, respectively. The exchange from H^+ to Na^+ leads to a homogenization of the first ligands shell around Ti: the average Ti–O distance remains similar, but the standard deviation decreases for pentacoordinated (model D, 1.91±0.09 Å) and hexacoordinated (model F, 1.99±0.09 Å) models. A detail of the local geometry of the Ti in each model is displayed in Figures S2-S8. The experimental UV-vis spectra of TS-1A and TS-1B samples are compared to the simulated ones for the seven cluster models in Figure 2.

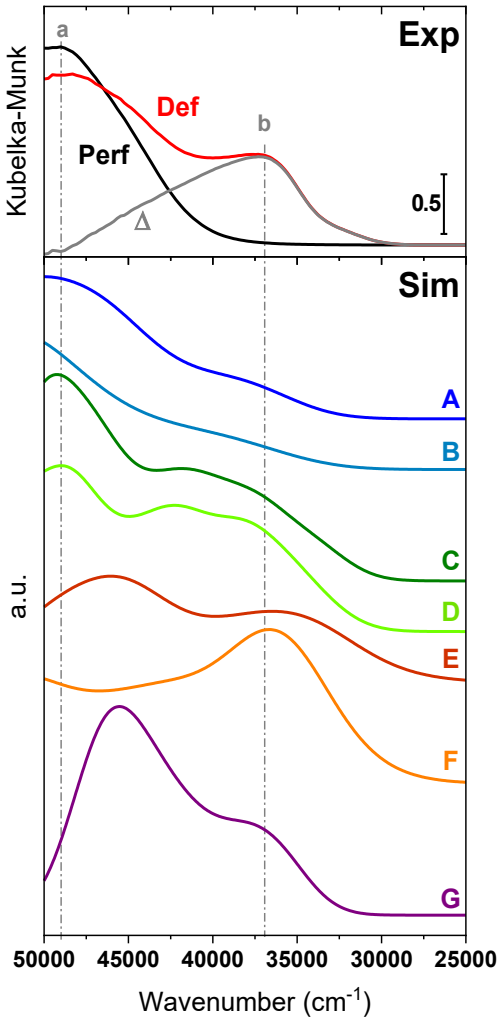

Figure 2. In the top panel (Exp), experimental UV-vis spectra for the perfect TS-1A (Perf) and the defective TS-1B (Def) samples. A difference spectrum Δ is calculated subtracting the contribution of perfect sites from TS-1A from the spectrum of TS-1B, weighted on the perfect Ti concentration (i.e. Δ = Def – 0.89·Perf). In the bottom panel (Sim), simulated UV-vis spectra for the seven models reported in Figure 1: A, perfect tetracoordinated Ti; B, bipodal tetracoordinated Ti; C, H-terminated pentacoordinated Ti; D, Na-terminated pentacoordinated Ti; E, H-terminated hexacoordinated Ti; F, Na-terminated hexacoordinated Ti; and G, dimeric tetracoordinated Ti.

The optical spectrum of the perfect TS-1A sample is characterized by a single band peaking at around 48000 cm^{-1} (feature *a* in Figure 2), assigned to the LMCT typical of tetrahedral Ti.[22,23] For the defective TS-1B material, a second band is observed at 37000 cm^{-1} (labeled as *b* in Figure 2), assigned in the literature to the electronic fingerprint of various type of defective Ti species, generally to hexacoordinated Ti belonging to the MFI framework[13] or forming non-framework structures.[15,24] This feature is highlighted in the difference spectrum Δ, further exhibiting an asymmetric tail toward higher wavenumbers. By comparing experimental and computational results, the simulated spectrum for the perfect tetrahedral Ti structure (model A) nicely matches with the experimental one from TS-1A, emphasizing the reliability of the simulation method here adopted. Trying to assign the transition at 37000 cm^{-1} to a specific structure, the only model that can be univocally excluded is the bipodal tetrahedral Ti (model B). All the other structures exhibit intense absorptions in the 30000-40000 cm^{-1} range. However,

the most prominent one belongs to the Na-terminated hexacoordinated Ti (model F), nicely matching the position and the profile of the experimental signal. Nevertheless, also other models could explain the defect transition, although they all show their major features at higher energies, in some cases overlapping with the LMCT of tetrahedral Ti. Noteworthy, none of the proposed structures exhibit bright electronic transitions at wavenumber lower than 30000 cm^{-1}, where experimental signals are usually ascribed to extended TiO_2 particles.[25,26]

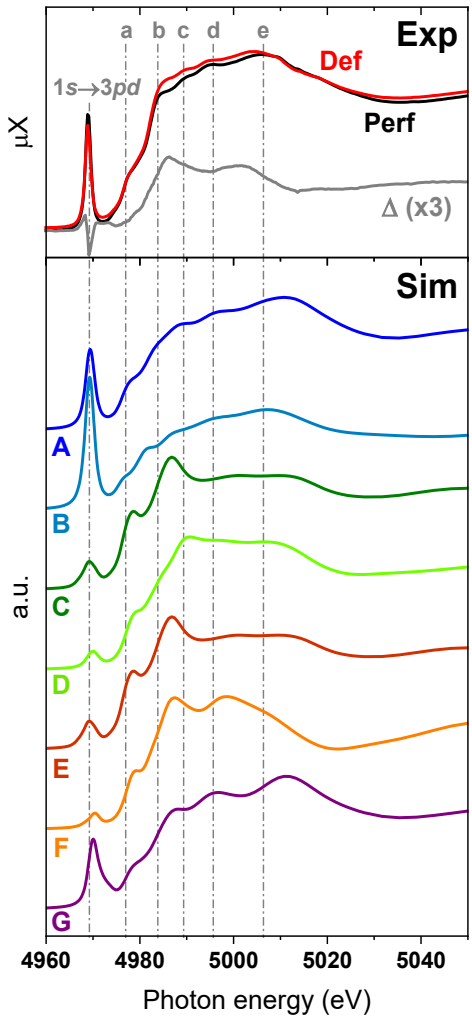

Figure 3. In the top panel (Exp), experimental Ti K-edges XANES spectra for the perfect TS-1A (Perf) and the defective TS-1B (Def) samples. A difference spectrum Δ is calculated subtracting the contribution of perfect sites from TS-1A from the spectrum of TS-1B, weighted on the perfect Ti concentration (i.e. Δ = Def – 0.89·Perf, multiplied by a factor 3 for the sake of visualization). In the bottom panel (Sim), the simulated Ti K-edges XANES spectra for the seven models reported in Figure 1: A, perfect tetracoordinated Ti; B, bipodal tetracoordinated Ti; C, H-terminated pentacoordinated Ti; D, Na-terminated pentacoordinated Ti; E, H-terminated hexacoordinated Ti; F, Na-terminated hexacoordinated Ti; and G, dimeric tetracoordinated Ti.

Figure 3 shows Ti K-edges XANES measured on the two samples and their weighted difference Δ, compared to ones simulated on the proposed structural models. Despite XAS is usually referred as a bulk/averaging technique, in this specific case we can use it to identify specific structures thanks to the monodispersed nature of the local environments of Ti in our samples (including only perfect tetrahedral

sites in TS-1A and perfect + well-defined defective sites in TS-1B, as we discussed in a previous work[2]). The most distinctive feature in TS-1 XANES spectra is the intense pre-edge peak assigned to the Ti *1s* $\rightarrow$ *3pd* electronic transition, peaked at 4969 eV, characteristic of the tetrahedral Ti species.[27–29] Its intensity is directly proportional to the concentration of perfect tetrahedral Ti. Accordingly, the intensity ratio of the pre-edge peak of TS-1B over TS-1A (equal to 0.89) matches the ratio of their perfect tetrahedral Ti sites concentrations (see Table 1). The simulated data on this specific feature will not be discussed here, since the finite difference method used in FDMNES is not suitable for correctly describing core-to-valence electronic transitions. Thereby, DFT based simulations have been performed to give a methodologically correct simulation of the pre-edge feature: these data are shown in Figure S9 of SI and discussed herein. Conversely, we assessed our simulation method appropriately describes the edge region, on the basis of benchmark calculations for reference materials (TiO_2 and ETS-10, see Figure S10 and comments herein). Instead, a detailed comment on the articulated features characterizing the edge region of TS-1 XANES spectra is missing in the literature. Some preliminary results showed that such region is highly affected by the local environment of perfect tetrahedral Ti,[30] then significant differences are expected changing the ligand spheres around the absorbing atom. In the XANES spectrum of TS-1A five distinct features are observed at 4977, 4984, 4989, 4996 and 5006 eV, labeled as *a*, *b*, *c*, *d* and *e* in Figure 3, respectively. For TS-1B, closely the same features are observed with some minor variations (in agreement with the low percentage of defective sites over the total amount of Ti, in the order of 10%, see Table 1): the intensity of features *b* and *c* is higher, and these two components become less resolved than in the spectrum of TS-1A. Furthermore, the maximum of the broad *e* component is found at lower energies, resulting from the slight dephasing of the first EAXFS oscillation, which is anticipated in the case of TS-1B. These differences are well-distinguished in the weighted difference spectrum Δ, where a new peak is found at 4986 eV, between the *b* and *c* features, and the anticipation of the *e* feature at 5000 eV is evident.

By comparing experimental and simulated spectra, the perfect tetracoordinated Ti model A is able to correctly reproduce the five features characterizing the edge region of the TS-1A XANES spectrum. Nevertheless, also the simulated spectra for models B (bipodal tetracoordinated Ti) and G (dimeric tetracoordinated Ti) show a similar profile. In the simulations for higher coordination Ti sites (models C-F), instead, distinctive fingerprints are observed, specifically two defined peaks falling just above the energy of the *a* feature and between *b* and *c* ones, respectively. The latter could be the cause of the increased intensity of the *b*, *c* features in the TS-1B XANES spectrum. The higher energy one also nicely matches the most intense feature as observed in the weighted difference spectrum Δ for models C, E and F. Furthermore, in the sole case of model F (Na- terminated hexacoordinated Ti), the *e* feature is found at lower energies compared to the other simulated spectra; in overall, the simulated spectrum for model F is qualitatively very similar to the weighted difference spectrum Δ. Thereby, the comparison of experimental and simulated Ti K-edge XANES spectra suggests that the defective sites characterizing the TS-1B sample are most probably hexacoordinated Ti centers, with a local symmetry approaching the octahedral one. This datum enforces the previous findings from UV-vis.

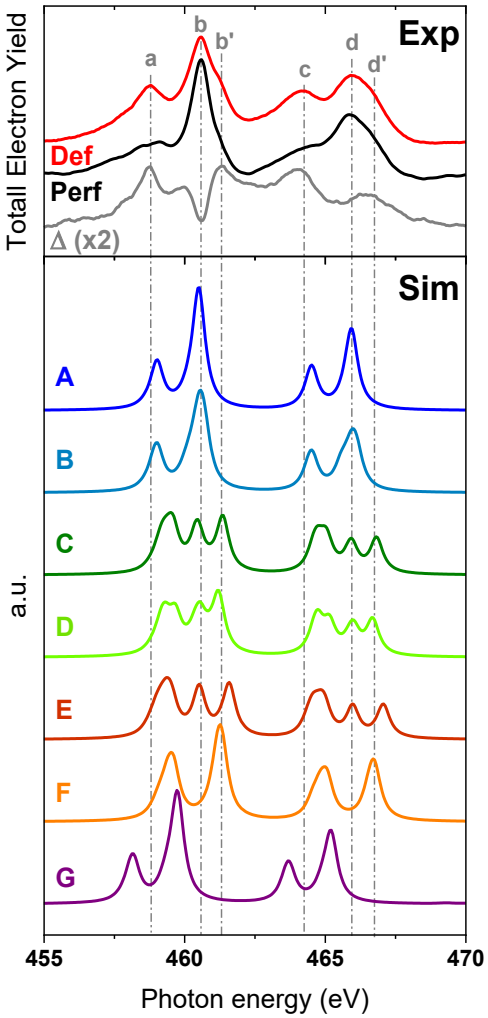

Figure 4. In the top panel (Exp), experimental Ti $L_{2,3}$-edges NEXAFS spectra for the perfect TS-1A (Perf) and the defective TS-1B (Def) samples. A difference spectrum Δ is calculated subtracting the contribution of perfect sites from TS-1A from the spectrum of TS-1B, weighted on the perfect Ti concentration (i.e. Δ = Def – 0.89·Perf, multiplied by a factor 2 for the sake of visualization). In the bottom panel (Sim), the simulated Ti $L_{2,3}$-edges NEXAFS spectra for the seven models reported in Figure 1: A, perfect tetracoordinated Ti; B, bipodal tetracoordinated Ti; C, H-terminated pentacoordinated Ti; D, Na-terminated pentacoordinated Ti; E, H-terminated hexacoordinated Ti; F, Na-terminated hexacoordinated Ti; and G, dimeric tetracoordinated Ti.

The experimental Ti $L_{2,3}$-edges NEXAFS spectra of TS-1A and TS-1B, shown in Figure 4, display similar fingerprints but having significantly different relative intensities, as further highlighted in their weighted difference spectrum Δ. The spectrum of TS-1A is characterized by four peaks, labeled *a* (458.8 eV), *b* (460.6 eV), *c* (464.1 eV) and *d* (466.0 eV), being the *b* and *d* components much more intense than the *a* and *c* ones. The position in energy of these features, as well as their relative intensities, agrees with those previously reported for TS-1.[14] This pattern of bands can be assigned to the $2p_{3/2} \rightarrow 3d$ (*a, b*) and $2p_{1/2} \rightarrow 3d$ (*c, d*) transitions of Ti in a tetrahedral ligand environment, according to the crystal field theory (CFT). In the defective TS-1B sample, the relative intensity of peaks *a, c* vs *b, d* remarkably increases and additional shoulders are observed at 461.3 and 466.8 eV (labeled *b'* and *d'*, respectively). Based on

CFT, the additional signals observed in the spectrum of TS-1B can be related to a larger splitting of the *3d* orbitals, ascribable to the presence of different Ti centers with higher coordination. In detail, we can estimate that the splitting of the *3d* orbitals increases from the 1.8 eV characterizing the perfect sites in TS-1A to the 2.5 eV for defects in TS-1B, as obtained from the difference in energy of features *b*-*a* and *b'*-*a*, respectively. By comparing the experimental with simulated spectra, as for the previous techniques, the perfect tetracoordinated structure model (A) correctly reproduces the features of the TS-1A sample. The bipodal tetracoordinated model (B) shows a similar pattern as well, with a slight broadening of the peaks which derives from the inequivalence of the ligands surrounding Ti. The dimeric model (G), despite its tetracoordinated ligand environment around each absorbing atom, is not matching the experimental data, neither in the case of the defective TS-1B sample. For this reason, we can exclude the presence of dimeric species in these materials. The penta- and hexa-coordinated models are instead characterized by features clearly distinguishing them from the tetracoordinated ones: the models C-E exhibit a triplet of peaks for both the L_2 and L_3 edges, whereas model F has a shape similar to that of perfect Ti, but having relative intensities closer to those experimentally observed for TS-1B. Comparing the simulated spectra to the weighted difference spectrum Δ, relevant similarities are found with the simulated spectrum for model F: an optimal match of features *b'* and *d'* (i.e. ones more representative for the defect sites in TS-1B) is observed; the same level of confidence is not achieved in terms of energy for the features *a* and *c*, however a good agreement is recognized considering their relative intensities vs those of signals *b'*, *d'*. Due to the broadness of the difference spectrum signals, we cannot completely exclude the presence of other Ti sites with a higher coordination (penta- or hexa-coordinated). However, by taking in account the outcomes of UV-vis and XANES, there are strong evidences of the closely octahedral nature of the defective Ti sites. In order to counter check our assignment, we performed a fit of the Ti k-edge EXAFS of our samples, as described in detail in Section S6 of SI and depicted by Figures S11-S13. Briefly, we first fitted the EXAFS of TS-1A adopting model A as structural representation of the perfect tetrahedral Ti sites, then we performed a biphasic fit of the EXAFS of TS-1B by using again the model A (and the parameters derived in the first fit) to describe the perfect Ti, whereas we chose model F (Na-terminated hexacoordinated Ti) to depict Ti defects. All the obtained parameters are provided in Table 2. Interestingly, the biphasic fit of TS-1B, provided a fraction of defects *1-x* contributing to the EXAFS equal to 8% of total Ti. This datum, also accounting for the complexity of the fit (whose quality is however good, as testified by the reasonable R-factors, see also Figure S12), nicely matches the compositional analysis we reported in a previous paper[2] and here recalled in Table 1, supporting our structural assignment for Ti defective sites. Also the other fitted parameters yielded meaningful values, in particular the expansion coefficients α and β, associated to the structural models A and F, we adopted to represent the perfect tetrahedral Ti and the defective Ti, respectively: the proximity of these values to 1 (i.e. unaltered model) again confirms the validity of our structural hypothesis.

Table 2. Best-fit values of the parameters optimized in the EXAFS fits for the TS-1A and TS-1B spectra: the weight of the perfect tetrahedral Ti site component on the overall EXAFS spectrum (x), the amplitude scattering factor (S_0^2), the Debye Waller factors for O in perfect (σ_{Operf}^2) and defective (σ_{Odef}^2) Ti sites, the energy shift (ΔE) and the expansion coefficient for the for the structural models adopted to describe perfect (model A, coefficient α) and defective (model F, coefficient β) Ti sites. The R-factors, reporting for the goodness of the fit, are shown as well. The fits were performed in the R space over the 1.0–2.8 Å interval on the $k^2\chi(k)$ function Fourier-transformed in the 2.4–14.5 $Å^{-1}$ k-space interval. Fixed parameters are underscored without the corresponding errors. The parametrized variables were 4 over 15 independent for the TS-1A and TS-1B respectively.

	x	S_0^2	σ_{Operf}^2 ($Å^2$)	σ_{Odef}^2 ($Å^2$)	ΔE (eV)	α	β	R-factor
TS-1A	<u>1</u>	0.92 ± 0.05	0.002±0.001	-	1.8 ± 0.7	0.998± 0.003		0.016
TS-1B	0.82 ± 0.12	<u>0.92</u>	<u>0.002</u>	0.01±0.01	<u>1.8</u>	<u>0.998</u>	0.98± 0.04	0.019

Conclusion

This work reports an unprecedented systematic study on possible defective Ti sites in TS-1, providing a library for the electronic features of several hypothetical Ti structures. In particular, the comparison of three distinct spectroscopic observables allows overcoming the typical weakness of electronic spectroscopies in pin-pointing the precise structure of the observed centers. The coupling of spectroscopies with simulation has been proved to be central for our purposes, since the lack of appropriate reference materials would have hampered the achievement of the detailed assignment here presented. The evidences from experiments, rationalized on the basis of simulation results, infer that the defective sites characterizing our sample (but commonly reported in several studies) are hexacoordinated Ti sites embedded in the MFI framework, with a local symmetry approaching the octahedral one. Despite the simplified model adopted for the description of Ti defects, e.g. not accounting for the possible structural heterogeneity of defective sites and for the presence of a small fraction of anatase in TS-1B, we obtained a remarkable agreement between experimental and simulated data. The valuable structural insight here obtained will allow depicting more accurately the catalytic role of defects in TS-1 in partial oxidation reactions, described since now on the basis of barely qualitative considerations.

Acknowledgements

This work was pushed since the beginning and strongly desired by our beloved Carlo Lamberti, to whom we will be forever grateful for his teachings and for his inexhaustible energy, so appreciated during the tiring synchrotron measurements. MS, VC, SB and FB acknowledge Evonik Resource Efficiency for the lively support to this research. The authors acknowledge the CERIC-ERIC Consortium and Elettra Sincrotrone Trieste for the access to experimental facilities and financial support. We are grateful to our colleagues and friends Alessandro Piovano and Andrea Martini for their valuable contribution during the NEXAFS experiments and for the development and testing of the software for the NEXAFS data reduction. The simulations were performed on resources provided by UNINETT Sigma2 - the National

Infrastructure for High Performance Computing and Data Storage in Norway, under project number NN9381K. The Italian ministry of University and Research is acknowledged for financial support through the PRIN 2107 program (project 2017KKP5ZR). LB and PT acknowledge Nanoscience Foundry and Fine Analysis (NFFA-MIUR Italy Progetti Internazionali) facility.

Keywords: Titanium Silicalite-1; defects; UV-vis; K-edge XAS; L-edges XAS; DFT

References

[1] B. Notari, G. Perego, M. Taramasso, *Preparation of Porous Crystalline Synthetic Material Comprised of Silicon and Titanium Oxides*, **1983**, US4410501 A.

[2] M. Signorile, V. Crocellà, A. Damin, B. Rossi, C. Lamberti, F. Bonino, S. Bordiga, *J. Phys. Chem. C* **2018**, *122*, 9021–9034.

[3] F. Schmidt, M. Bernhard, H. Morell, M. Pascaly, *Chem. Today* **2014**, *32*, 31–35.

[4] V. Russo, R. Tesser, E. Santacesaria, M. Di Serio, *Ind. Eng. Chem. Res.* **2014**, *53*, 6274–6287.

[5] V. Russo, R. Tesser, E. Santacesaria, M. Di Serio, *Ind. Eng. Chem. Res.* **2013**, *52*, 1168–1178.

[6] C. Neri, B. Anfossi, A. Esposito, F. Buonomo, *Process for the Epoxidation of Olefinic Compounds*, **1984**, US4833260 (A).

[7] P. Roffia, M. Padovan, E. Moretti, G. De Alberti, *Catalytic Process for Preparing Cyclohexanone-Oxime*, **1988**, US 4745221 (A).

[8] P. Roffia, G. Leofanti, A. Cesana, M. Mantegazza, M. Padovan, G. Petrini, S. Tonti, P. Gervasutti, in *Stud. Surf. Sci. Catal.*, **1990**, pp. 43–52.

[9] A. C. Alba-Rubio, J. L. G. Fierro, L. León-Reina, R. Mariscal, J. A. Dumesic, M. López Granados, *Appl. Catal. B Environ.* **2017**, *202*, 269–280.

[10] J. C. Van Der Waal, M. S. Rigutto, H. Van Bekkum, *Appl. Catal. A Gen.* **1998**, *167*, 331–342.

[11] L. J. Davies, P. McMorn, D. Bethell, P. C. B. Page, F. King, F. E. Hancock, G. J. Hutchings, *J. Catal.* **2001**, *198*, 319–327.

[12] A. Wróblewska, M. Rzepkowska, E. Milchert, *Appl. Catal. A Gen.* **2005**, *294*, 244–250.

[13] Q. Guo, K. Sun, Z. Feng, G. Li, M. Guo, F. Fan, C. Li, *Chem. - A Eur. J.* **2012**, *18*, 13854–13860.

[14] Y. Zuo, M. Liu, T. Zhang, L. Hong, X. Guo, C. Song, Y. Chen, P. Zhu, C. Jaye, D. Fischer, *Rsc Adv.* **2015**, *5*, 17897–17904.

[15] J. Su, G. Xiong, J. Zhou, W. Liu, D. Zhou, G. Wang, X. Wang, H. Guo, *J. Catal.* **2012**, *288*, 1–7.

[16] M. G. Finn, K. Barry Sharpless, *J. Am. Chem. Soc.* **1991**, *113*, 113–126.

[17] M. Signorile, A. Damin, F. Bonino, V. Crocellà, G. Ricchiardi, C. Lamberti, S. Bordiga, *J. Phys. Chem. C* **2018**, *122*, 1612–1621.

[18] M. Signorile, A. Damin, F. Bonino, V. Crocellà, C. Lamberti, S. Bordiga, *J. Comput. Chem.* **2016**, *37*, 2659–2666.

[19] M. W. Anderson, O. Terasaki, T. Ohsuna, A. Philippou, S. P. MacKay, A. Ferreira, J. Rocha, S. Lidin, *Nature* **1994**, *367*, 347–351.

[20] V. Bolis, S. Bordiga, C. Lamberti, A. Zecchina, A. Carati, F. Rivetti, G. Spanò, G. Petrini, *Microporous Mesoporous Mater.* **1999**, *30*, 67–76.

[21] C. Lamberti, S. Bordiga, D. Arduino, A. Zecchina, F. Geobaldo, G. Spano, F. Genoni, G. Petrini, A. Carati, F. Villain, G. Vlaic, *J. Phys. Chem. B* **1998**, *102*, 6382–6390.

[22] M. R. Boccuti, K. M. Rao, A. Zecchina, G. Leofanti, G. Petrini, *Stud. Surf. Sci. Catal.* **1989**, *48*, 133–144.

[23] F. Geobaldo, S. Bordiga, A. Zecchina, E. Giamello, G. Leofanti, G. Petrini, *Catal. Letters* **1992**, *16*, 109–115.

[24] Q. Guo, Z. Feng, G. Li, F. Fan, C. Li, *J. Phys. Chem. C* **2013**, *117*, 2844–2848.

[25] H. Tang, F. Lévy, H. Berger, P. E. Schmid, *Phys. Rev. B* **1995**, *52*, 7771–7774.

[26] A. Amtout, R. Leonelli, *Phys. Rev. B* **1995**, *51*, 6842–6851.

[27] D. Gleeson, G. Sankar, C. Richard A. Catlow, J. Meurig Thomas, G. Spanó, S. Bordiga, A. Zecchina, C. Lamberti, *Phys. Chem. Chem. Phys.* **2000**, *2*, 4812–4817.

[28] S. Bordiga, F. Boscherini, S. Coluccia, F. Genonic, C. Lamberti, G. Leofanti, L. Marchese, G. Petrini, G. Vlaic, A. Zecchina, *Catal. Letters* **1994**, *26*, 195–208.

[29] R. J. Davis, Z. Liu, J. E. Tabora, W. S. Wieland, *Catal. Letters* **1995**, *34*, 101–113.

[30] A. A. Guda, S. A. Guda, K. A. Lomachenko, M. A. Soldatov, I. A. Pankin, A. V. Soldatov, L. Braglia, A. L. Bugaev, A. Martini, M. Signorile, E. Groppo, A. Piovano, E. Borfecchia, C. Lamberti, *Catal. Today* **2019**, *336*, 3–21.